Multiscale and multispectral characterization of mineralogy with the ExoMars 2020 rover remote sensing payload

Allender, E.j.; Cousins, C.r.; Gunn, M.d.; Caudill, C.m.

Published in:
Earth and Space Science

DOI:
10.1029/2019EA000692

Publication date:
2020

Citation for published version (APA):
Allender, E. J., Cousins, C. R., Gunn, M. D., & Caudill, C. M. (2020). Multiscale and multispectral characterization of mineralogy with the ExoMars 2020 rover remote sensing payload. *Earth and Space Science*, *7*(4), [e2019EA000692]. https://doi.org/10.1029/2019EA000692

Earth and Space Science

RESEARCH ARTICLE
10.1029/2019EA000692

Key Points:
- ExoMars imaging suite effectively detects and characterizes science targets across multiple scales
- Spectral parameter suite distinguishes crosscutting vein features, mudstones, and oxidization states
- Cross-referencing of multiscale datasets allows generation of detailed stratigraphic sections

Supporting Information:
- Supporting Information S1

Correspondence to:
E. J. Allender,
ea63@st-andrews.ac.uk

Citation:
Allender, E. J., Cousins, C., Gunn, M., & Caudill, C. (2020). Multiscale and multispectral characterization of mineralogy with the ExoMars 2020 rover remote sensing payload. *Earth and Space Science*. 7, e2019EA000692. https://doi.org/10.1029/2019EA000692

Received 29 APR 2019
Accepted 29 JAN 2020
Accepted article online 3 FEB 2020

Multiscale and Multispectral Characterization of Mineralogy with the ExoMars 2020 Rover Remote Sensing Payload

E. J. Allender[1], C. R. Cousins[1], M. D. Gunn[2], and C. M. Caudill[3]

[1]School of Earth and Environmental Sciences, University of St Andrews, St Andrews, UK, [2]Department of Physics, Aberystwyth University, Penglais Campus, Aberystwyth, UK, [3]Centre for Planetary Science and Exploration (CPSX), University of Western Ontario, London, Ontario, Canada

Abstract In 2020, the European Space Agency and Roscosmos will launch the ExoMars rover, with the scientific objective to detect evidence of life within the Martian surface via the deployment of a 2 m drill. The ExoMars Pasteur payload contains several imaging and spectroscopic instruments key to this objective: the Panoramic Camera (PanCam), Infrared Spectrometer for ExoMars (ISEM), and Close-UP Imager (CLUPI). These instruments are able to collect data at a variety of spatial (sub-mm to decimeter) and spectral (3.3 to 120 nm) resolutions across the 440 to 3,300 nm wavelength range and collectively will form a picture of the geological and morphological characteristics of the surface terrain surrounding the rover. We deployed emulators of this instrument suite at terrestrial analog sites that formed in a range of aqueous environments to test their ability to detect and characterize science targets. We find that the emulator suite is able to effectively detect, characterize, and refine the compositions of multiple targets at working distances spanning from 2 to 18 m. We report on (a) the detection of hydrothermal alteration minerals including Fe-smectites and gypsum from basaltic substrates, (b) the detection of late-stage diagenetic gypsum veins embedded in exposures of sedimentary mudstone, (c) multispectral evidence of compositional differences detected from fossiliferous mudstones, and (d) approaches to cross-referencing multi-scale and multi-resolution data. These findings aid in the development of data products and analysis toolkits in advance of the ExoMars rover mission.

1. Introduction

In 2020, the European Space Agency (ESA) and the Russian Space Agency (Roscosmos) will deliver the ExoMars rover *Rosalind Franklin* and surface platform to the surface of Mars, whose communications with Earth will be supported by the already operational ExoMars Trace Gas Orbiter (TGO). The ExoMars rover Pasteur payload (Barnes et al., 2006; Vago et al., 2017) contains a suite of nine instruments plus a subsurface drill, which will be used to address ExoMars' primary objective of detecting evidence of extinct life within subsurface deposits (McMahon et al., 2018; Vago et al., 2017). Among these are a number of imaging instruments, including the Panoramic Camera (PanCam) (Coates et al., 2017) and the CLose UP Imager (CLUPI) (Josset et al., 2017), with point hyperspectral data provided by the Infrared Spectrometer for ExoMars (ISEM) (Korablev et al., 2017). The ExoMars rover will be the first mission to combine imagers covering three different spatial scales (including stereo; Barnes et al., 2018) in combination with a point infrared spectrometer, in situ at the Martian surface. This combination presents a huge range of potential data products with which to investigate the geology along the rover traverse.

Data from PanCam, ISEM, and CLUPI will augment existing, coarser-resolution orbital information (The ExoMars 2018 Landing Site Selection Working Group (LSSWG), 2014) with multiscale observations of surface morphology, color, texture, grain size, and compositional information to provide the environmental context for tactical and strategic planning operations and support the prioritization of drilling locations where pristine subsurface material can be accessed.

Ancient terrains record a history of aqueous activity and subsequent alteration. Noachian (>3.7 Ga) terrains in particular grant access to an epoch of deposits no longer available for study on Earth (Nimmo & Tanaka, 2005). As prolonged, aqueous Martian environments may have been habitable to microorganisms (Vago et al., 2017), we deployed instrument emulators in areas hosting minerals which had formed

in a range of aqueous environments to assess potential science targets. These areas included large-scale sedimentary depositional systems (Torrey, Utah, USA; Tjörnes, Iceland) and systems displaying authigenic low-temperature alteration of basalt (Námafjall, Iceland) that host deposits of phyllosilicates, sulfates, zeolites, and iron oxides (Harris et al., 2015; Michalski et al., 2010; Murchie et al., 2009).

We explore the utility of the PanCam, ISEM, and CLUPI data product suite for detecting terrain characteristics (including composition, morphology, texture, grain size, weathering and oxidation state, hydration state, size, and color) at multiple scales. From this multispatial and spectral scale information obtained from exposures at the surface mineralogical targets and paleoenvironmental history can be established. We show that the instrument suite is able to support the astrobiological goals of the ExoMars mission by revealing hydrated mineralogy, second-order alteration, and the extrapolation of compositional features across the wider terrain, aiding long-term mission planning.

1.1. Instrument Emulators

The ExoMars Pasteur payload is described in detail in Vago et al. (2017). Throughout this paper, we refer to the combination of PanCam, CLUPI, and ISEM emulators as the ExoMars emulator suite. These instruments and their emulators provide color, multispectral, and hyperspectral information at multiple scales within a single scene. Cross-calibration of their data pre-launch will aid in the interpretation of mineralogy and potential science targets in the primary science phase of the mission.

1.1.1. Panoramic Camera (PanCam)

PanCam data will provide local scale morphological and mineralogical context along the rover traverse (Coates et al., 2017). The ExoMars PanCam's heritage comes from the Beagle 2 Stereo Camera System (Griffiths et al., 2005) and from the National Aeronautics and Space Administration's (NASA) Mars Exploration Rover (MER) Pancams (Bell et al., 2003). PanCam is composed of two wide angle cameras (WAC) set 50 cm apart, which image a 38.3° field of view (FOV) across a 440–1,000 nm spectral range, and a single high-resolution camera (HRC, described below). An 11-space filter wheel within each WAC comprises three broadband color filters, six narrowband geology filters, and two solar filters. PanCam RGB imaging differs from that of Mastcam (Malin et al., 2010) (onboard NASAs Mars Science Laboratory (MSL) rover *Curiosity*) and Mastcam-Z (Bell et al., 2016) (onboard NASAs upcoming Mars2020 rover mission) in that PanCam uses these broadband color filters instead of RGB Bayer filters (Bell et al., 2016; Wellington et al., 2017). PanCam emulator data are provided by the Aberystwyth University PanCam Emulator 3 (AUPE3), which has been built with off-the-shelf components to replicate ExoMars PanCam specifications as closely as possible and is designed for use in Mars analog terrains (Harris et al., 2015). When deployed, AUPE3 is mounted on an optical bench (alongside ISEM-E and HRC-E) 2 m above the ground to replicate its position on the ExoMars mast. The FOV of AUPE3 is 34° , slightly smaller than that of PanCam, and in place of the PanCam solar filters in positions 10 and 11, there is a luminance filter covering the visible portion of the spectrum and an empty filter slot for panchromatic imaging (Harris et al., 2015). Details of the filter wheels in Left WAC (LWAC) and Right WAC (RWAC) cameras for AUPE3 versus the ExoMars PanCam are provided in Table 1. For both AUPE3 and PanCam, a 6-band multispectral file is generated from each LWAC or RWAC geology filters, which can be merged to produce a 12-band multispectral file spanning 440–1,000 nm. A smaller 3-band multispectral file is produced by the RGB broadband filters for either WAC. While the spectral filters differ between ExoMars PanCam and MER Pancam (Cousins et al., 2012), PanCam builds on a wealth of existing data regarding image processing (e.g., Alexander et al., 2006; Bell et al., 2004, 2004b, 2004c; Barnes et al., 2011, 2011; Farrand et al., 2006, 2008, 2013, 2014; Parente et al., 2009). To correct raw image data to relative reflectance, a Macbeth ColorChecker© is used in tandem with this instrument to emulate the calibration target to be positioned on ExoMars' deck (Barnes et al., 2011).

1.1.2. High-Resolution Camera (HRC)

HRC is a color camera system that will investigate rock textures in high resolution from the rover's working distance. HRC is located inside the PanCam optical bench next to the RWAC. Both HRC and its emulator HRC-E are able to capture high-resolution subset images of the larger PanCam FOV; their FOVs are 4.88° and 5.45° , respectively. HRC pixels measure approximately 0.17 mm at a rover working distance of 2 m and 8.5 cm per pixel at a distance of 1 km (Coates et al., 2017). At the time this work was undertaken HRC-E was simply monochromatic (see Figure 3a) but at the time of publication it has been updated to more closely resemble the flight model which uses a Bayer filter pattern to capture color imagery. RGB color provided by HRC will closely represent RGB color captured with PanCam as both will be calibrated with observations of the calibration target located on Rosalind Franklins deck.

Earth and Space Science

10.1029/2019EA000692

Table 1
Filter Wheel Specifications for AUPE3 and ExoMars PanCam (Cousins et al., 2012; Coates et al., 2017)

		AUPE3				ExoMars PanCam	
		LWAC	RWAC			LWAC	RWAC
Filter #	Filter	Center wavelength (FWHM)	Center wavelength (FWHM)	Filter #	Filter	Center wavelength (FWHM)	Center wavelength (FWHM)
1	Blue Broadband	440 (120)	440 (120)	1	Blue Broadband	440 (120)	440 (120)
2	Green Broadband	540 (80)	540 (80)	2	Green Broadband	540 (80)	540 (80)
3	Red Broadband	640 (100)	640 (100)	3	Red Broadband	640 (100)	640 (100)
4	Geology 1	438 (24)	740 (13)	4	Geology 1	440 (25)	740 (15)
5	Geology 2	500 (24)	775 (25)	5	Geology 2	500 (20)	780 (20)
6	Geology 3	532 (10)	850 (25)	6	Geology 3	530 (15)	840 (25)
7	Geology 4	568 (10)	900 (25)	7	Geology 4	570 (12)	900 (30)
8	Geology 5	610 (10)	950 (50)	8	Geology 5	610 (10)	950 (50)
9	Geology 6	671 (10)	1000 (50)	9	Geology 6	670 (12)	1000 (50)
10	Visible	545 (290)	545 (290)	10	Solar 1	925 (5)	450 (5)
11	Empty	Panchromatic	Panchromatic	11	Solar 2	935 (5)	670 (5)

Note. WAC filter bandpasses are given as full width at half maximum (FWHM) values. Units are nanometers.

1.1.3. Infrared Spectrometer for Mars (ISEM)

Mounted below PanCam is the Infrared Spectrometer for ExoMars (ISEM) (Korablev et al., 2017). This instrument provides point spectra for a 1° FOV within the larger PanCam FOV and the 4.88° FOV of HRC. ISEM uses an acousto-optic tunable filter (AOTF) to cover a spectral range from 1,150 to 3,300 nm at variable resolution. It is projected that one ISEM spectrum will be captured per HRC image. Targeting of HRC and ISEM will be driven by the discovery of mineralogical and morphological features of interest observed in PanCam imagery. Combining all of these instruments allows detailed analysis of diagnostic mineral features in the VNIR to SWIR wavelengths. For the ISEM emulator, ISEM-E, we use a handheld field spectrometer (Spectral Evolution RS-3500) with a spectral range of 350–2,500 nm and a spectral resolution of 3 nm. When in contact with the outcrop, the ISEM-E FOV is approximately 1 cm. While ISEM will not share any overlapping spectral bands with PanCam, the overlap of ISEM-E and AUPE3 allows for spectral comparison between these two instruments.

1.1.4. Close-Up Imager (CLUPI)

Mounted on the drill of ExoMars 2020 is the CLose-UP Imager (CLUPI) (Josset et al., 2017). CLUPI is a high-resolution, color camera system designed to mimic what a geologist would observe in the field through a hand lens, providing images of minerals within their original context before they are powdered for geochemical analyses. Such high-resolution data will facilitate the search for morphological features that may indicate biosignatures on outcrops and drill cores and provide grainsize constraints for sedimentary material. When at a distance of 10 cm from a target, CLUPI provides 7 micron per pixel resolution with an FOV of 1.9×1.3 cm. CLUPI uses a Foveon X3 detector which captures all RGB color information at the same spatial location, so, unlike detectors which use a Bayer filter, the resulting image data do not require any interpolation. CLUPI color images will closely represent RGB color from PanCam's filter set and will additionally be calibrated using the CLUPI calibration target located near the drill box (Josset et al., 2017). The CLUPI emulator CLUPI-E is a Sigma SD15 Digital SLR which uses the same detector as the CLUPI instrument. The lens is a Sigma 100 mm macro lens which provides a representative field of view and magnification range.

2. Geological Settings

Oxia Planum is the selected landing site for the ExoMars rover (European Space Agency, 2018). The landing ellipse for this site contains phyllosilicate-rich layered region which is overlain by a deltaic sedimentary fan, indicative of the ponding of water post-dating the layered formation (Quantin-Nataf et al., 2018). Later stage volcanic activity has partially covered the layered clay deposits. The entire region has been heavily eroded since these units were emplaced (The ExoMars 2018 Landing Site Selection Working Group (LSSWG), 2014). As a consequence, ExoMars will likely encounter hydrated mineral terrains along its traverse and both sedimentary and volcanic deposits. The ability of the ExoMars emulator suite to characterize geological targets is explored using four terrestrial analog sites, each described in detail below. These field sites were selected as they encompass aspects of Noachian clay-bearing sites and late Noachian to early Hesperian alluvial deposits, as well as a variety of other geological features relevant to ExoMars preparation. For the purposes of instrument testing they also had a scant vegetation coverage, (b) well-characterized geology, and (c) access to mains power. They were not specifically chosen to be analogous to locations where subsurface life has been preserved, as PanCam, ISEM, and CLUPI are not specifically designed to identify biosignatures.

2.1. Námafjall, Iceland

Námafjall is a geothermal field in the central northern region of Iceland (65° 38′26.5″N, 16° 48′43.2″W) (Figure 1a). We focus on Námafjall ridge, which has exposures of subglacially erupted basalts displaying various stages of weathering and hydrothermal alteration. The first ("Pillow") is extensively weathered, with oxidized soils surrounding its base, dark glass-rich quench rinds, and small (1–5 cm) secondary zeolite deposits dispersed throughout. The second outcrop ("Pillow_Alt") is also weathered and has additionally undergone extensive secondary alteration and displays crosscutting gypsum veins. These outcrops were previously imaged with an earlier iteration of AUPE3 in Harris et al. (2015) as A07_Pillow and A08_Veins, respectively. These deposits in combination with their alteration phases provide an example of low-temperature (<150 ° C) neutral-acidic alteration of basaltic material. The light-toned veins are also analogous to calcium sulfate veins detected on Mars at Endeavour and Gale craters (e.g., Arvidson et al., 2014; Grotzinger et al., 2014; Nachon et al., 2014; Squyres et al., 2012).

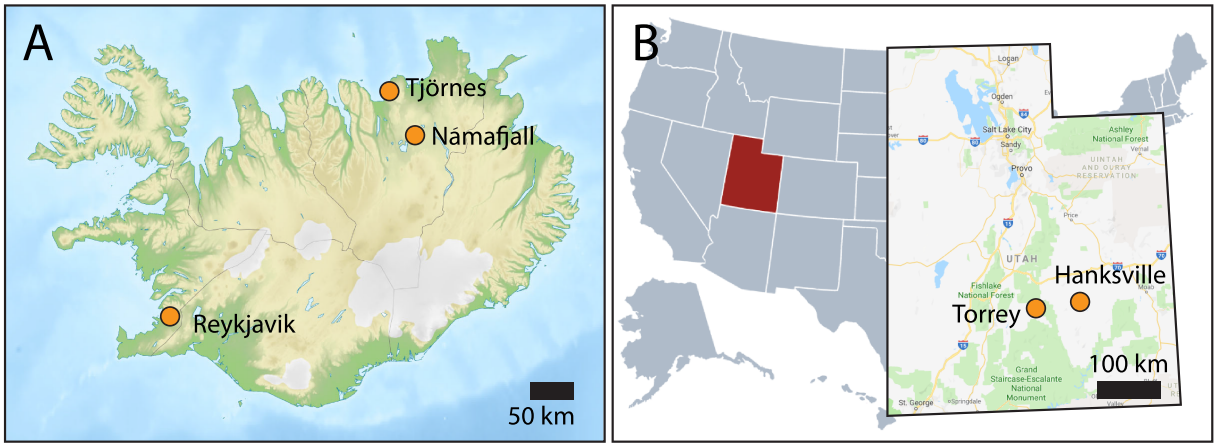

Figure 1. (a) Locations of Icelandic field sites (with the exception of Reyjavik, which is shown only for reference). (b) Locator map for the United States with Utah shown in red. Inset map shows Utah field sites.

2.2. Tjörnes, Iceland

Tjörnes is located in northern Iceland at Kaldakvísl (66° 6′18.1″N, 17° 16′58.3″W, Figure 1a) where the Tjörnes sedimentary beds sit on a tertiary basalt formation. This section contains the Tapes layer, the oldest and lowest layer of the Tjörnes beds. The Tjörnes sediments here are formed of fossiliferous marine sediments (Einarsson, 1994). Fluvial and lacustrine beds, as well as brown coal, are interspersed, providing an example of deposits that formed in a transitional, shallow water depositional environment. In particular, these sediments have a basaltic source, making them geochemically comparable to Martian sediments (Cannon et al., 2015), in contrast to quartzofeldspathic sediments more typically found in terrestrial systems.

2.3. Torrey, USA

The Triassic Moenkopi formation in southern Utah, USA, is characterized by mudstone interbedded with siltstone, sandstone, and gypsum beds that represent tidal marginal marine and sabkha environments at the edge of the Early Triassic epeiric sea (Young & Chan, 2017). We deploy the ExoMars emulator suite at an exposure near 38° 18′05″N, 111° 29′11.7″W, just outside the towns of Torrey and Teasdale, UT (Figure 1b). This site is included as a terrestrial analog as the formation is crosscut by light-toned gypsum veins analogous to the calcium sulfate veins detected on Mars at Endeavour and Gale craters (e.g., Arvidson et al., 2014; Grotzinger et al., 2014; Nachon et al., 2014; Squyres et al., 2012).

2.4. Hanksville, USA

Alluvial deposits here are preserved as inverted channels in the Brushy Basin and Salt Wash Members of the Jurassic Morrison Formation and the Ruby Ranch member of the Cretaceous Cedar Mountain Formation (Williams et al., 2011) in the Hanksville region (38° 22′12″N, 110° 42′36″W, Figure 1b). The inverted channel imaged at this site provides an example of vertical stratigraphy able to be imaged from a rover perspective. The outcrop is weathered and is composed generally of red and green mudstones with a sandstone capping unit containing layers with multiple grain sizes. Some mineral veins and large conglomerates are visibly embedded in the lower mudstones. We use this site to illustrate the multiscale capabilities of the instrument emulator suite and to capture mudstones exhibiting different oxidation states.

3. Methodology

3.1. Field Methodology

The emulator suite was deployed at each field site at a working distance of 2–18 m from each outcrop: At this distance the spatial resolution was 1.2–10.8 mm per pixel. A Macbeth ColorChecker© was placed in front of the outcrop when capturing the scene to enable radiometric calibration post-imaging. We assume both the MacBeth ColorChecker and the outcrop surface are Lambertian scatterers, and to ensure that both were imaged under the same illumination conditions, with the same geometry and at approximately the same time, the Macbeth ColorChecker was positioned such that it had approximately the same local incidence/emission angles as the targeted features. For Námafjall and Tjörnes weather conditions were overcast, resulting in uniform lighting conditions. For the Utah sites, skies were generally clear with bright sunlight;

Table 2
Spectral Parameters Calculated for AUPE3 Within ExoSpec

Name	Description	Rationale
LWAC		
S438_671	[(R671-R438)/(671-438)]	Related to degree of oxidation
BD532	[1-(R532/((0.53*R500)+(0.47*R568)))]	Identifies ferric minerals, particularly hematite, and is related to degree of oxidation
BD610	[1-(R610/((0.6*R568)+(0.4*R671)))]	Can indicate goethite development and can be influenced by olivine and pyroxene
S532_610	[(R610-R532)/(610-532)]	Ferric minerals and dust
R671_438	[R671/R438]	Ferric minerals and dust
S610_671	[(R671-R610)/(671-610)]	Tests for presence of shoulder absorption indicative of hematite or goethite
RWAC		
R740_1000	[(R740/R1000)]	Ferrous minerals
S740_1000	[(R1000-R740)/(1000-740)]	Strength and position of NIR absorption linked to ferrous minerals
BD775	[1-(R775/((0.5*R740)+(0.545*R850)))]	Nontronite
BD900	[1-(R900/((0.455*R840)+(0.545*R950)))]	Strength of NIR absorption, related to ferric minerals
S900_1000	[(R1000-R900)/(1000-900)]	Related to detection of hydrous minerals
BD950	[1-(R950/((0.5*R900)+(0.5*R1000)))]	Related to hydrous minerals, some clays, and silicates
S950_1000	[(R1000-R950)/(1000-950)]	Linked to detection of hydrous minerals

however, passing clouds meant that lighting conditions were variable while AUPE3 data were being collected, resulting in RWAC spectra having to be omitted for the Hanksville site. We replaced this wavelength range with data from ISEM-E ground truth spectra. The timing of image collection depended on the direction that outcrops were facing; for example, east-facing outcrops were typically imaged in the morning while the sun was low and directly illuminating their faces to minimize overhead shadow. After outcrops had been imaged with AUPE3 and HRC-E, ISEM-E was used in handheld mode to collect point spectra of geologic features. In handheld mode, ISEM-E is held against each feature while its internal light source illuminates the surface, collecting and averaging 30 individual spectra to provide a final result, with an FOV around 1 cm. CLUPI-E was used to collect close-range, high-resolution images of each of these point spectra locations so that their exact sampling locations could be found in AUPE3 and HRC-E images. Finally, CLUPI-E was used to collect images for high-resolution mosaics to assist in visualization of the field site, and these were taken from the same working distance as AUPE3.

3.2. Processing Methodology

For each camera position in an AUPE3 mosaic two images were captured: one LWAC and one RWAC. All raw images were processed to R* reflectance defined by Reid et al. (1999) using the ExoMars Spectral Analysis Tool (ExoSpec) developed by Allender et al. (2018). ExoSpec performs flat-fielding, radiometric correction, and correction from radiance to R* reflectance using the in-scene Macbeth ColorChecker©. As the target and surface were imaged with approximately the same geometry and at approximately the same time, we assume they are imaged under the same illumination conditions and so do not consider corrections for diffuse versus direct illumination. However, work to compensate for differences in viewing geometry between a rover mounted horizontal calibration target and a variable geometry outcrop is underway and will be incorporated into a future version of ExoSpec. Following correction to R* reflectance, ExoSpec generates spectral parameter maps for both LWAC and RWAC (Table 2). Spectral parameter maps enable band depths and shoulders to be visualized, which can indicate broad mineralogical composition, abundance, or grain size fluctuations. These parameters have proven effective for the MER Pancams (Farrand et al., 2006, 2008, 2013, 2014, 2016; Rice et al., 2010, 2013) and for orbital imagers like the Compact Reconnaissance Imager for Mars (CRISM) (Pelkey et al., 2007; Viviano-Beck et al., 2014). We experimented with RGB color combinations and different spectral parameter maps to determine which combination best highlights specific geologic features depending on the challenges posed by each field site. Note that none of the spectral parameters listed in Table 2 are *diagnostic* of specific minerals, rather they test for features consistent with absorptions that indicate the presence of some minerals. For example, the S610_671 parameter tests for the presence of the 650 nm hematite shoulder feature, but other ferric oxides such as goethite also have similar absorptions (610 nm) that light up this parameter. Similarly, some (but not all) hydrated minerals have a negative slope from 950 to 1,000 nm, but Fe-bearing minerals with broad absorptions at around 1,000 nm may have a negative slope as well.

To confirm the presence of different compositional units at each site we also performed decorrelation stretches to highlight RGB color differences (Gillespie et al., 1986), principal components analyses to locate unique spectral classes at each outcrop, and outlier detection with the Reed-Xiaoli Detector (RXD) algorithm (Reed & Yu, 1990) to locate pixels which differ significantly from the average global spectral response of an image in order to highlight potential science target locations (Figure 4); see supporting information for the results for all sites. We examined these images alongside the spectral parameter maps for spatial agreement. All the above visualization steps were performed on AUPE3 data in order to assess the overall spectral diversity of each scene. Next, AUPE3 spectra were extracted from regions of interest (ROI) highlighted in these images and compared to the ISEM-E spectral data. Each ROI typically contained a minimum of 50–100 spatially contiguous pixels. As an example, assuming an AUPE3 working distance of 4 m, an ROI containing 50 pixels will cover a region of approximately 1.2 by 1.2 cm, which is comparable to the ISEM-E FOV of 1 cm. The mean signature from each ROI was considered its representative, and standard deviation was also computed in order to quantify variation within each ROI. Cross-referencing AUPE3 with ISEM-E datasets allowed a greater spectral range (438–2,500 nm) to be examined for diagnostic absorption features.

Bulk mineralogy for the Torrey and Hanksville sites was characterized by X-ray diffraction (XRD). The samples were disaggregated from rock (or sediment/powder) and ground with an agate mortar and pestle. To preserve the original grain size and mineral structure, approximately 20 g of material of each sample was ground and sifted through a 500 μm sieve. The randomly oriented fine powder was front-packed onto glass slides and analyzed at the Laboratory for Stable Isotope Science (The University of Western Ontario) using a high-brilliance Rigaku Rotaflex RU-200B series X-ray diffractometer, equipped with a rotating anode (Co K-α source operated at 160 mA and 45 kV) and a graphite monochromator. Scans were performed from 2 to 82° 2θ at a step size of 0.02° 2θ. Analysis was performed using the QualX phase identification program for powder diffraction data (Altomare et al., 2008). XRD pattern peaks were compared to standard XRD mineral patterns from the POW_COD Crystallography Open Database (Downs & Hall-Wallace, 2003; Grazulis et al., 2009, 2012). Quantitative analyses ("S-Quant") were additionally performed within QualX via reference intensity ratios (RIR) based on the standard chosen from the mineral database.

4. Results

4.1. Crosscutting Mineral Features

Outcrops at Iceland (Pillow, Altered Pillow, and Tjörnes) and Utah (Torrey) all feature either high-albedo crosscutting mineral veins (Pillow, Altered Pillow, and Torrey) or discrete carbonate mineral features (Tjörnes), which were used to investigate the utility of the ExoMars emulator suite in the detection and characterization of high-albedo, hydrated mineral deposits. Here, targets were analyzed with radiometrically corrected AUPE3 true color imaging, false color imaging—using S532_610, R671_438, and BD610 as RGB—and ISEM-E spectra (Figure 2). Additional AUPE3 multispectral products investigated (Figure 4) include the outlier detection using the Reed-Xiaoli Detector (RXD) algorithm, PCA false color combinations, the ratio between red and blue wavelengths (R671_438), and the negative slope between the 950 and 1,000 nm filters (S950_1000). Products for all sites are provided in supporting information.

The Pillow outcrop was imaged with AUPE3 at a working distance of 4 m, resulting in a spatial resolution of 2.4 mm per pixel. The RGB image (Figure 2a) reveals low-albedo glass-rich quench rinds, light-toned mineral deposits varying from 1 to 5 cm in width dispersed across the pillow basalt outcrop that do not conform to any pre-existing structural features, an oxidized weathered surface that dominates the majority of the outcrop, and light-toned soils. These are represented here by four spectral units. The ISEM-E spectrum of the light-toned mineral deposit (Figure 2e) has a doublet feature at 2,300–2,350 nm, which can be the result of Mg substituting for Fe in the Mg/Fe-OH combination (Viviano-Beck et al., 2014). The ISEM-E spectrum of the mineral deposit within the basalt matrix (red spectrum in Figure 2e) displays small absorption features around 2,200 and 2,300 nm. Possible interpretations of mineralogical composition of these spectra include nontronite, zeolite (analcime/heulandite), calcite, and palagonite, which are also all products of low-temperature (<150 ° C) hydrothermal alteration of volcanic substrate and possess similar absorption features in the VNIR/SWIR (Cloutis et al., 2002; Warner & Farmer, 2010). Light-toned amygdaloidal mineral deposits can be visualized at a higher-spatial resolution with CLUPI-E and are approximately 1 mm in size given the spatial resolution (<5 mm per pixel) at an imaging distance of 40 cm (Figures 3b and 3c). Bulk mineralogy results at this site from Harris et al. (2015) suggest the presence of calcite, smectite, Fe-oxide, plagioclase, and stilbite, while VNIR/SWIR results confirm the presence of zeolite and nontronite.

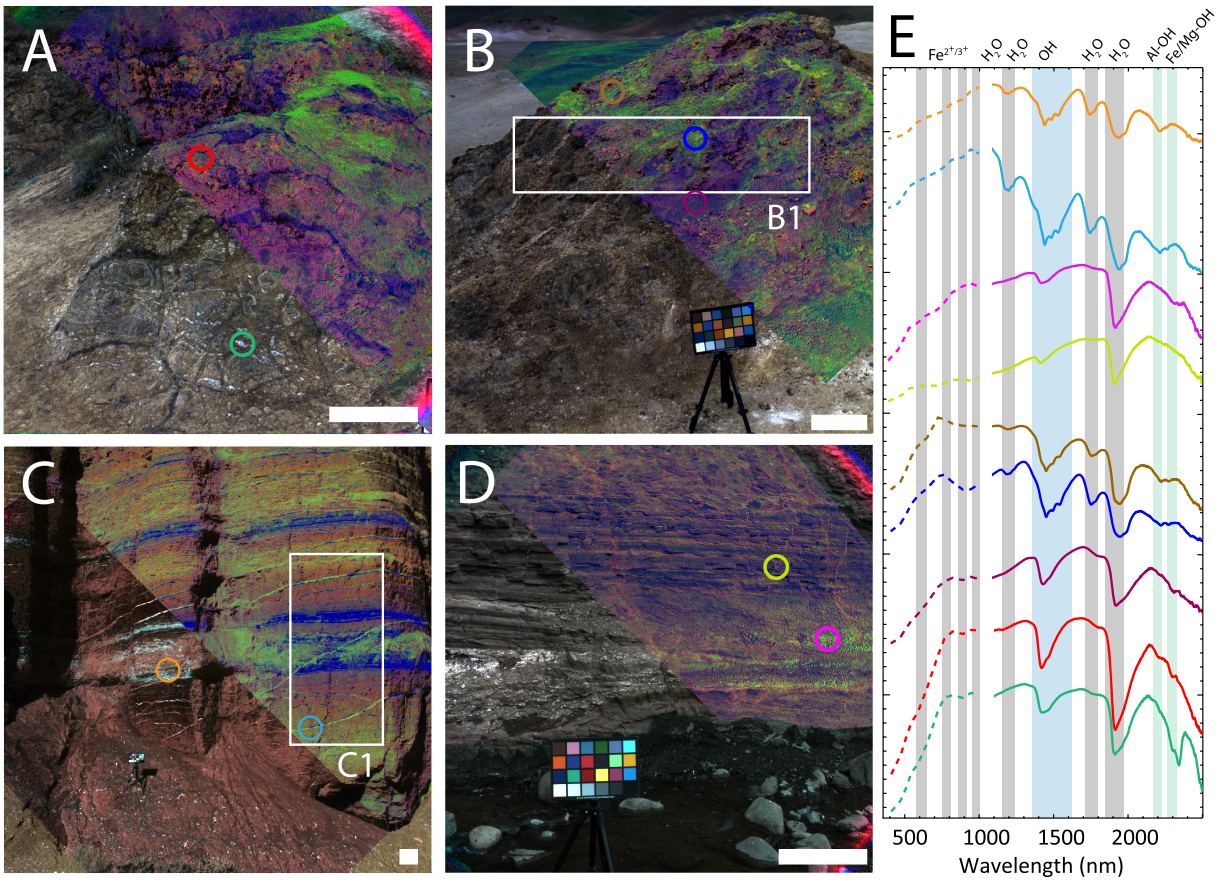

Figure 2. Detection of crosscutting high-albedo mineral features showing an AUPE3 true color composite in bottom-right of each image and a band depth composite in the upper-left. All composite images are constructed using S532_610, R671_438, and BD610 as RGB, respectively. Colored circles depict regions from which AUPE3 and ISEM-E spectra have been taken. Scale bar = 20 cm. (a) Pillow outcrop, Iceland. (b) Altered Pillow outcrop, Iceland. Macbeth ColorChecker is visible. (B1) HRC-E coverage region for Figure 3a. (c) Torrey outcrop, USA. (C1) This region is displayed using an additional spectral parameter in Figure 4C1. (d) Tjörnes outcrop, Iceland. (e) AUPE3 and ISEM-E spectra from each of the colored circles in (a–d), with absorption bands marked.

The Altered Pillow outcrop was imaged with AUPE3 at a distance of 3 m, resulting in a spatial resolution of 1.8 mm per pixel. Light-toned mineral veins crosscut the outcrop which has eroded to form light-toned soil in the image foreground (Figure 2b); these are consistent with the false color green spectral unit seen in the Pillow outcrop (Figure 2a). The S950_1000 summary parameter captures the edge of the hydration feature at around 1,000 nm (Rice, Bell III et al. 2013; Rice, Cloutis et al. 2013) for these features (supporting information). Spectra extracted from targeted regions in Figure 2b are shown in Figure 2e. The mineral vein has well-defined gypsum absorption features in its ISEM-E spectrum and possesses a negative 950–1,000 nm slope in PanCam multispectral data, which is in agreement with observations of gypsum by MER Pancam (Farrand et al., 2014, 2016). The altered light material is a mix of eroded gypsum and the oxidized substrate material, as shown by the presence of a broad band centered around 900 nm. This negative slope across the 950–1,000 nm range is not apparent in the Fe-rich gypsum signature due to the presence of a broad Fe^{2+} 900 nm band obscuring this feature. Fine-scale structures and grain sizes can be visualized with HRC-E. An HRC-E image is shown in Figure 3a for the region indicated within Figure 2B1. Bulk mineralogy results for light-toned soils along Námafjall ridge from Harris et al. (2015) suggest the presence of gypsum, plagioclase, smectite, zeolite, hematite, and goethite; and VNIR/SWIR results confirm the presence of these (Figures 2e and 9).

The Torrey outcrop was measured with AUPE3 at a working distance of 18 m, resulting in a spatial resolution of 10.8 mm per pixel. In the false color AUPE3 image (Figure 2c), green pixels highlight both the crosscutting veins and the dried red unit, which is likely a result of the gypsum veins weathering out to disperse a fine amount of material across the outcrop. The S950_1000 spectral parameter separates the veins from the other units (Figure 2C1, parameter result shown in Figure 4C1). Here, only veins are picked out using white pixels,

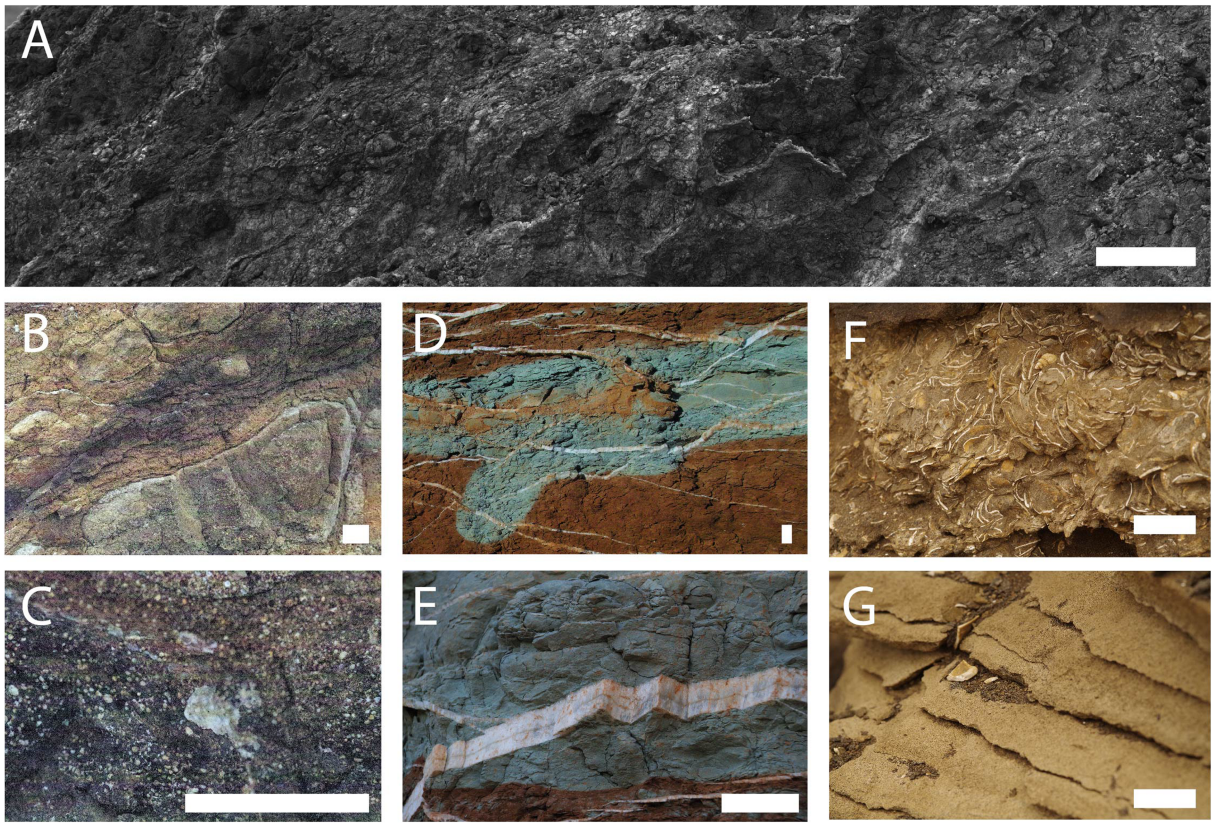

Figure 3. Multiscale and textural detail achievable with HRC-E and CLUPI-E. All scale bars = 5 cm. (a) HRC-E horizontal mosaic (comprised of 10 images, arranged in two rows of five) of Altered Pillow midsection from Figure 2b showing altered light material and weathered basaltic material. Based on this working distance (3 m) grain sizes are estimated to be <0.5 mm per pixel and are not resolvable. (b) CLUPI-E context image of Pillow showing dark glass-rich quench rind, grain sizes not resolvable at this resolution (<0.25 mm per pixel). (c) CLUPI-E image of amygdaloidal mineral deposits within Pillow which are estimated to be larger than 1 mm given this imaging distance (<0.05 mm per pixel at 40 cm). (d) CLUPI-E context image of Torrey showing red and green mudstones interlaced with mineral veins and overlain with dry red material; grain size of this mudstone is not resolvable at 0.57 mm per pixel. (e) CLUPI-E detail image of a gypsum vein crosscutting green mudstone. Crystalline structure within the vein can be observed, and mudstone substrate is confirmed by very small grain sizes (<0.11 mm) below the resolution of the camera at this imaging distance (approximately 1 m). (f) CLUPI-E detail image of calcite deposits within mudstone at Tjörnes. (g) CLUPI-E detail image of siltstone layers at Tjörnes; some grains are resolvable at this imaging distance (0.11 mm per pixel at 1 m).

due to their negative slope across the 950–1,000 nm range (Figure 2e). For comparison, Figure 4c shows that the spectral parameter R671_438 can highlight light-toned deposits but cannot discriminate hydrated veins from among these. CLUPI-E images depicting the Torrey geological units are shown in Figures 3d and 3e. From these it is clear that the veins are crosscutting secondary features, emplaced after the formation of the red and green mudstone units. The SWIR spectra of the high-albedo veins (Figure 2e) are consistent with that of gypsum (Young & Chan, 2017) and the 950–1,000 nm VNIR slope is truly indicative of a sharp absorption feature around 1,000 nm in the ISEM-E ground truth spectrum. The SWIR spectrum of the dry red coating material (Figure 2e) is also consistent with gypsum, showing that the mineral veins are weathering out and dispersing this material. Bulk mineralogy results for this site confirm the presence of gypsum, as well as calcite, quartz, illite, and smectite within the mudstones (see supporting information).

Finally, the cliff exposure at Tjörnes (Figure 2d) was measured with AUPE3 at a working distance of approximately 9 m, resulting in a spatial resolution of approximately 5.4 mm per pixel. Fractures are visible in places within the AUPE image, and lower strata exhibit a clear dip to one side. As with the Pillow and Altered Pillow outcrops (Figures 2a and 2b), the false color spectral parameter combination highlights the calcite layers in green and furthermore enables their fine banding patterns to be distinguished within the surrounding layers. CLUPI-E images depicting Tjörnes geological features at a higher-spatial resolution are shown in Figures 3f and 3g.

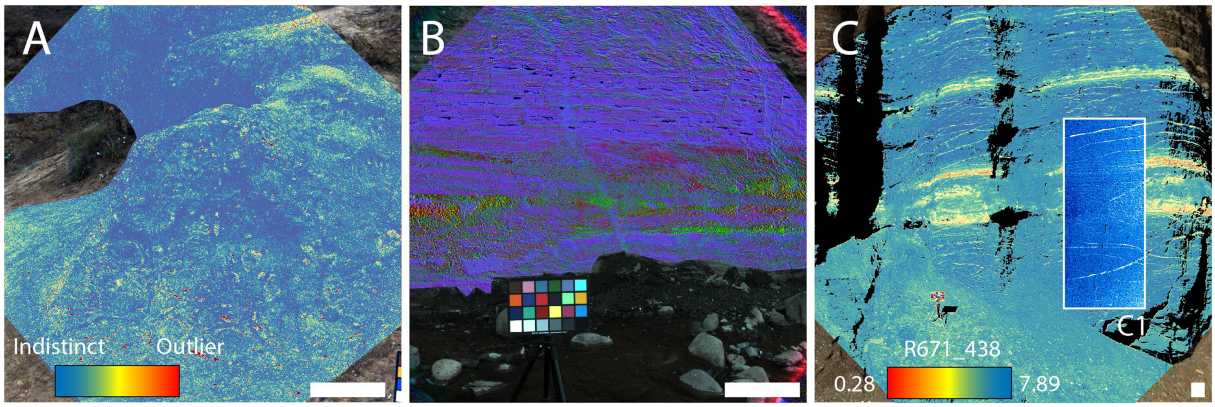

Figure 4. (a) RXD outlier detection result for Pillow outcrop. Red pixels represent outliers with respect to the average response of the image; here the light-toned mineral deposits are highlighted. (b) PCA analysis, overlying an AUPE3 true color image of Tjörnes. Calcite deposits are highlighted in green, and fine layering between dark and light mudstone units is also visible in blue and red. (c) AUPE3 summary parameter R671_438 highlights light-toned material (in yellow/red) at the Torrey site. (C1) Summary parameter S950_1000 isolating gypsum veins which are shown in white. All scale bars represent 20 cm.

4.2. Phyllosilicates and Mudstone

Within the Pillow outcrop, ISEM-E spectra refine the composition of surface materials to indicate the presence of Fe-smectite, in this case nontronite (Harris et al., 2015). Nontronite possesses non-diagnostic absorption features in the VNIR at around 450 nm (shoulder), 640 nm (absorption), and 940 nm (absorption), which are captured by AUPE3 (Figure 2e). In the associated SWIR spectra, absorption features occur at around 1,420, 1,910, 2,208, 2,290 nm, and at 2,410 and 2,510 nm (McKeown et al., 2018). These features

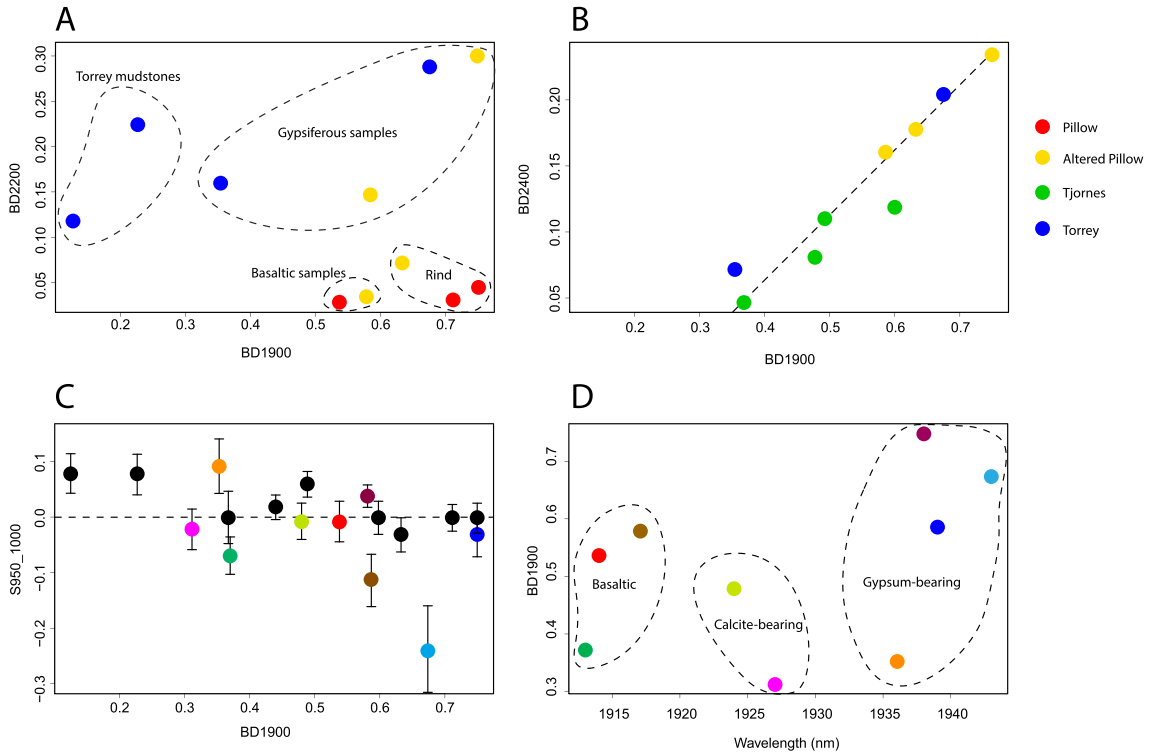

Figure 5. Error bars are not shown for ISEM measurements as they are smaller than the points used in the plot. (a) Spectral parameter plot of band depth at 2,200 nm versus the band depth at 1,900 nm. The mudstones at Torrey stand apart from the general data cluster, displaying smaller BD1900 values but high BD2200 values. No measurements at Tjörnes had absorption features at 2,200 nm. (b) Spectral parameter plot of BD2400 versus BD1900. A clear linear trend is apparent between these two parameters. (c) Plot of AUPE3 spectral summary parameter S950_1000 versus band depth at 1,900 nm by site. A negative S950_1000 value should indicate hydration. Colors for this plot correspond to spectra in Figures 2e and 9. (d) Plot of 1,900 nm absorption feature depth and wavelength shift indicating general composition regardless of site. Colors for this plot correspond to spectra in Figure 2e.

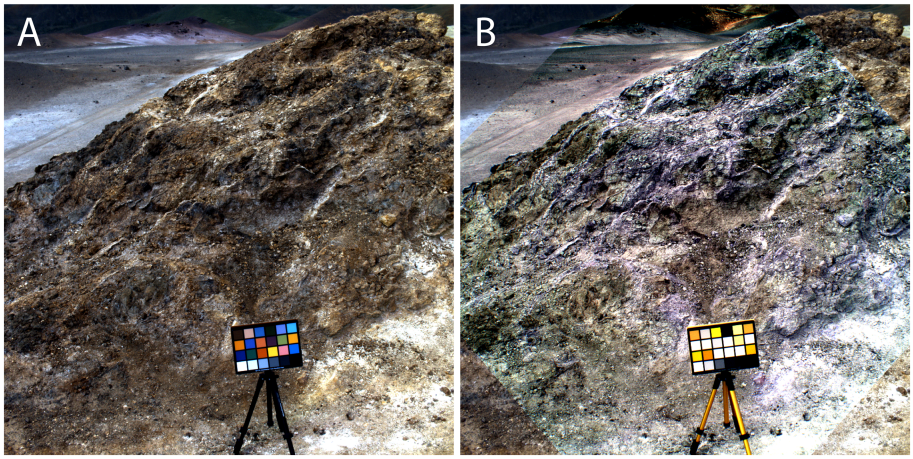

Figure 6. (a) AUPE3 RWAC true color RGB for visual comparison with (b). (b) AUPE3 RWAC composite with geology filters 6, 3, and 1 (1,000, 850, and 740 nm) assigned as RGB, respectively. Pixels which appear violet are indicative of Fe^{3+}-bearing mineralogy such hematite, which has an absorption feature at around 900 nm. Scale is given by the Macbeth ColorChecker© which is 21 cm in width.

are visible in ISEM-E spectra that were collected across the whole outcrop (Figure 9), suggesting pervasive alteration of this basalt. These VNIR and SWIR spectral features were also identified in AUPE3 and ISEM-E spectra for the basaltic substrate at the nearby Altered Pillow outcrop. Within the cliff exposure at Tjörnes, multispectral AUPE3 imaging delineated the darker and lighter strata (Figures 2d and 4b) beyond a simple difference in albedo: The darker sedimentary layers correspond to a deeper absorption at 610 nm, whereas the lighter-toned layers have a steeper slope between 438 and 610 nm (Figure 2e). HRC-E imaging results in images with 0.11 mm per pixel resolution, versus the 5.4 mm per pixel resolution provided by AUPE3 at this working distance. This resolution enables coarse-sand grain sizes to be resolvable (Figures 3f and 3g) and reveals fine-scale calcite deposits and sedimentary structures.

At the Torrey site (Figure 9) the red mudstone possesses weak hydration features, while those for the green mudstone are much stronger: Absorption features at around 2,200 and 2,300 nm suggest that this unit contains Mg-smectite. The mineral vein material is identified as gypsum (using the triplet absorption from 1,400 to 1,500 nm and absorption features at 1,750, 1,900, and 2,200 nm), while the dry red material possesses very similar, yet weaker, spectral features, supporting the idea that it is the result of a gypsum weathering process.

To assess the relationship between AUPE3 spectral parameters and ISEM-E hydration bands scatter plots were created using all ISEM-E spectral ROIs available in this study (Figure 5c). ISEM-E ROIs were not plotted if they possessed no absorption features at the plotted wavelengths. It is clear that all measurements possess a strong absorption feature at 1,900 nm regardless of the S950_1000 value, confirming that the S950_1000 spectral parameter alone is not a sufficient indicator of hydration state because most hydrated minerals do not exhibit their H_2O and/or OH absorptions in the correct location to produce this negative feature (Rice et al., 2010). There is a strong positive correlation between spectral parameters BD1900 and BD2400 (Figure 5b). The presence of absorption features at 1,900 and 2,400 nm can be indicative of zeolites, hydrated sulfates, and Al-phyllosilicates (Viviano-Beck et al., 2014). The shifting position of the 1,900 nm feature was also plotted with respect to its depth (Figure 5d). From this plot several data clusters are visible which correspond to their composition. The 1,900 nm versus 2,200 nm band depth effectively discriminates all targets (Figure 5a). The mudstones at Torrey stand apart from the general data cluster, displaying smaller BD1900 values but high BD2200 values.

4.3. Oxidation State

On top of, and surrounding, the Pillow outcrop are light-toned soils. These features are easily visible in both true and false color images of this outcrop in Figure 2a, where S532_610, S671_438, and BD610 are assigned as RGB, respectively. Using the same color mapping at Torrey, the image in Figure 2c is able to differentiate clearly between the red and green mudstone units and even shows detail in the fragmented materials in the sloping foreground.

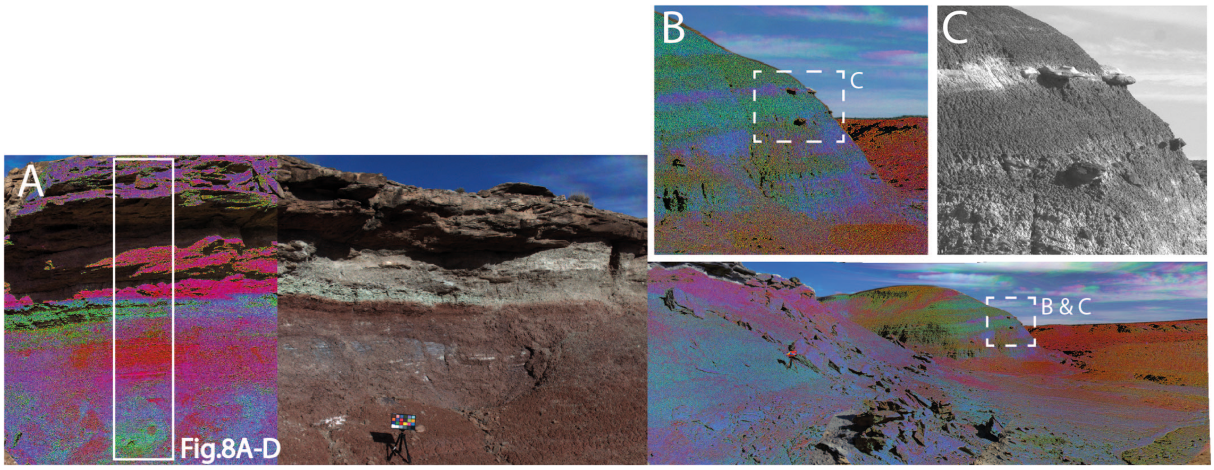

Figure 7. (a) AUPE3 mosaic showing oxidized and reduced clay units. Reduced clays are shown in magenta, highly oxidized units are shown in green, and oxidized units are shown in blue. For clarity, an RGB true color image is shown in the center of this mosaic. (b) Close-up of AUPE3 WAC image showing a distant mesa target, which illustrates that the green and magenta layers are spatially continuous from the layers shown in (a). (c) HRC-E of distant target (30 m away, 2.8 mm per pixel), allowing erosion-resistant sandstone units to be observed that were not resolvable at AUPE3 resolution. Scale in this image is given by the Macbeth ColorChecker© which is 21 cm in width.

Figure 6 illustrates that AUPE3 filter combinations can be used to refine oxidation state. Using RWAC filters at 1,000, 850, and 740 nm Fe^{3+}-bearing minerals such as hematite can be identified using the presence of an absorption feature at around 900 nm. This filter combination is based on MSL Mastcam's 1,012, 867, and 751 nm false color mosaic of Vera Rubin ("Hematite") Ridge (NASA, 2017).

The Hanksville outcrop was measured with AUPE3 at a working distance of approximately 4 m, resulting in a spatial resolution of approximately 2.4 mm per pixel (Figure 7a). The spectral parameter mosaic composed of parameters BD610, BD532, and S440_610 as RGB, respectively, highlights spectral diversity in the scene with respect to Fe-bearing minerals and highlights veins exposed within the outcrop. These features can be seen in more detail in Figure 8a–d.

4.4. Multiscale Utility

At Hanksville, the panchromatic HRC-E mosaic in Figure 8c refines the resolution imaged with AUPE3 to 0.37 mm per pixel at 4 m working distance and 2.8 mm per pixel at 30 m for distant observations (Figure 7c). CLUPI-E context images of these regions were also taken with a spatial resolution of 0.23 mm per pixel at 2 m working distance (Figure 8e) and 0.02 mm per pixel at approximately 20 cm working distance (Figure 8f). This range of resolutions allows potential strategic science targets at multiple distances to be investigated.

Combined AUPE3 RGB data, spectral parameter maps, and HRC-E textural and grain size information can define spectral and stratigraphic units (Figure 8d). An ISEM-E spectrum for each unit is displayed in Figure 8g. We also show bulk mineralogy (XRD) results for each of these units in Table 3. All units contain evidence for smectites, as indicated by their VNIR/SWIR spectral signatures in Figure 8g. The green coloring in green mudstone and smectite layers is produced by chlorite. Above the orange contact layer in Figure 8d, Table 3 shows all units contain evidence for gypsum.

5. Discussion

The ExoMars emulator suite was deployed at four field sites across Iceland and the United States and captured a range of geological information at multiple spectral and spatial resolutions. Data from this suite allow interpretation of surface outcrop characteristics like refined composition, morphology, texture, grain size, weathering and oxidation states, hydration state, size, and color. Furthermore, science targets, which may not be obvious in typical color images at a single scale, are able to be observed to a sub-cm level with this instrument combination.

5.1. Utility of AUPE3 Products Across Sites

The ExoMars rover PanCam, ISEM, and CLUPI emulator instruments were able to detect and confirm manually identified science targets at each site, as well as discover and refine the composition of others. Figure 9

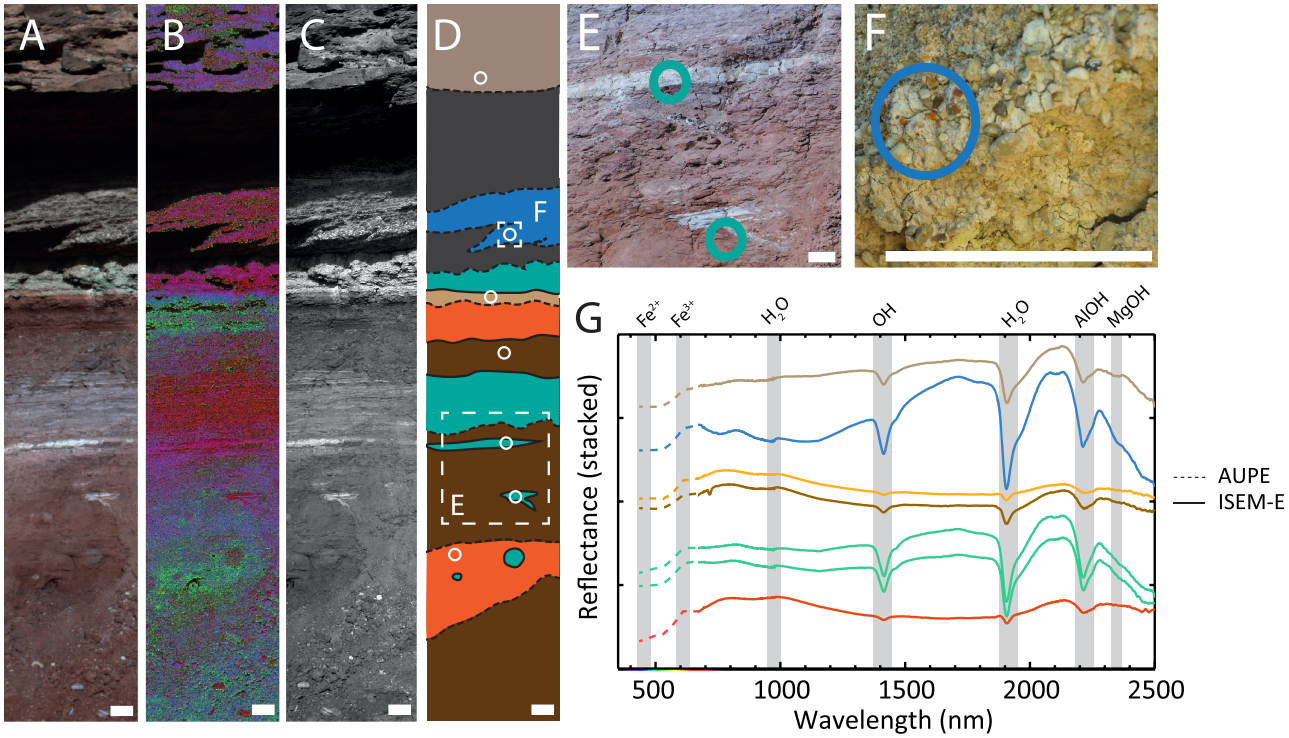

Figure 8. (a) AUPE3 RGB true color of inset strip from Figure 7a, spatial resolution is 2.4 mm per pixel: Grain sizes are not resolvable, but larger clasts can be seen. (b) AUPE3 false color parameter mosaic comprised of S532_610, S671_438, and BD610 as RGB, respectively, highlighting oxidized and reduced clay unit boundaries. (c) HRC-E mosaic illustrating that grain sizes and textures are able to be better resolved with this instrument (0.4 mm per pixel). (d) Stratigraphic log derived from the information in elements (a–c). Regions targeted with ISEM-E are shown with white circles. (e) CLUPI-E image of veins highlighted in AUPE3 and HRC-E images; green circles show locations targeted with ISEM-E. Imaged at 2 m (0.23 mm per pixel). (f) Sandstone/clay conglomerate imaged with CLUPI-E at a distance of 20 cm (0.02 mm per pixel). Blue circle shows the location targeted with ISEM-E. (g) AUPE3 and ISEM-E spectra taken from the locations specified in Figure 8d; colors correspond to their units given in that stratigraphic section. All scale bars = 10 cm.

shows AUPE3 and ISEM-E spectra of the science targets identified at each site; their spectral diversity widely varies depending on the type of aqueous environment. The spectra for the subglacially erupted site Pillow all exhibit features of the Fe-smectite nontronite, with varying albedos and oxidization states. Altered Pillow spectra exhibit features common to dark basalt and gypsum, as well as mixtures of varying oxidization state. Tjörnes spectra are flatter in the VNIR due to the low-albedo, gray material forming the Tapes beds;

Table 3
Bulk Mineralogy Results Derived From XRD Analysis for the Hanksville Stratigraphic Column

Unit description	Mineral 1	Mineral 2	Mineral 3	Mineral 4	Mineral 5	Mineral 6	Mineral 7
Dark red material	Illite/Smectite	Chlorite	Calcite	Quartz	Anatase		
Small vein	Quartz	Smectite	Chlorite	Calcite			
Large vein	Quartz	Smectite	Clinochlore	Illite	Ilmenite	Hematite	Magnesite
Light material	Smectite/Illite	Chlorite	Calcite	Quartz	Anatase		
Lamination	Quartz	Illite/Smectite	Ilmenite	Clinochlore	Hematite	Magnesite	
Dark red with green	Quartz	Smectite	Chlorite				
Dark brown material	Smectite/Illite	Chlorite	Calcite	Quartz	Anatase		
Beige gypsum contact	Illite/Smectite	Gypsum	Chlorite	Quartz	Anatase		
Green material	Illite/Smectite	Gypsum	Chlorite	Quartz	Anatase		
Conglomerate	Illite/Smectite	Chlorite	Quartz	Anatase			
Sandstone cap	Quartz	Gypsum	Smectite				

Note. Cell colors correspond to geological unit in Figure 8d.

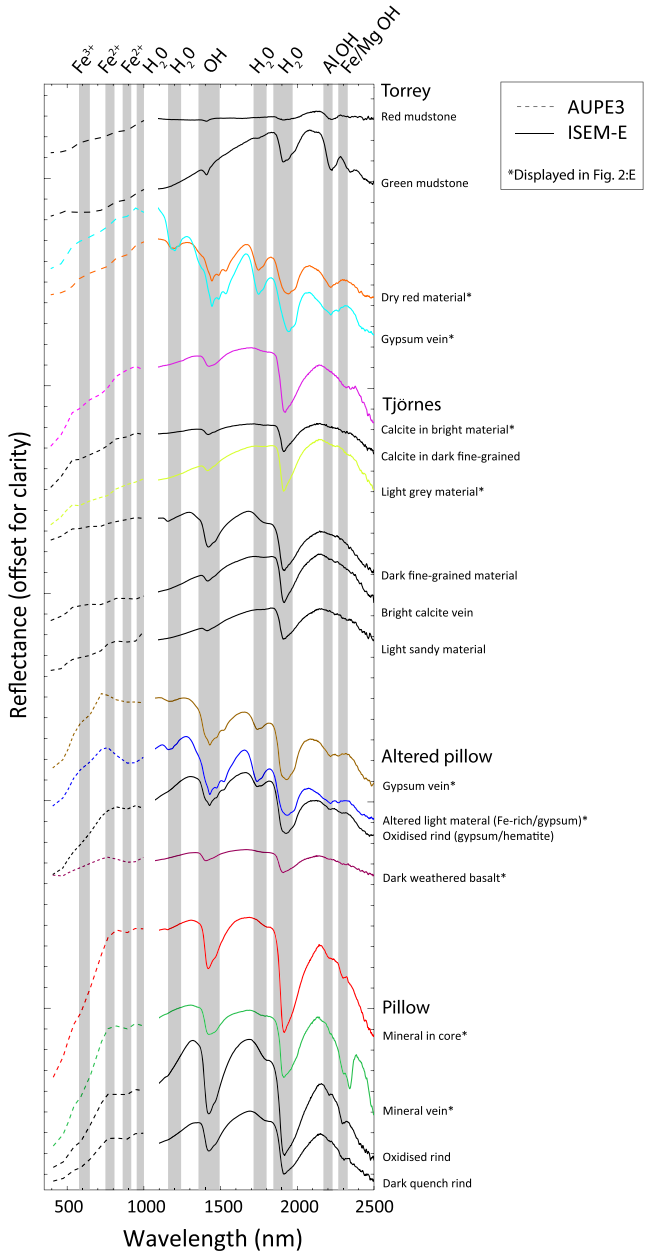

Figure 9. AUPE3 VNIR and ISEM-E SWIR spectra showing spectral diversity of samples at all sites. Colored spectra correspond to those in Figure 2e.

however, all possess hydration features at 1,400 and 1,900 nm in the SWIR. Here the dark fine-grained material spectrum possesses a deeper OH band around 1,400 nm, and a more defined 1,700 nm H_2O band than the other targets. The Torrey site spectra are very distinctively split between the mudstones and their secondary gypsiferous material, all of which would be suitable targets for the science goals of the ExoMars rover (Vago et al., 2017). The Hanksville inverted channel spectra all exhibit hydration features consistent with Al-smectite, which is confirmed in the XRD results from Table 3.

Figure 2 illustrates that spectral parameter combinations are loosely comparable across sites because they highlight units with similar characteristics (but not necessarily composition). For example, dark blue colors in Figure 2a and 2b both highlight dark basaltic material; however, in Figure 2a this is indicating quench rinds while in Figure 2b it is indicating substrate material. Likewise, green colors in Figure 2c and 2d indicate gypsiferous mineral veins and calcified deposits, respectively, while in Figure 2a they indicate light-toned

soils likely composed of nontronite. These units appear spectrally similar using this band combination and have different mineralogical compositions in the SWIR; however, the spectral parameter maps can only be used to highlight units with similar spectral characteristics at particular wavelengths in the VNIR and represent only broad compositional characteristics. A suite of parameter maps is useful to fully explore site diversity and can be used to guide ISEM-E pointing, expanding the wavelength range of AUPE3 into the SWIR and enabling diagnostic spectral features to be examined.

The Torrey gypsum veins and veins observed on Mars by Opportunity and Curiosity at Endeavour and Gale craters are late-stage diagenetic features that have experienced little alteration since emplacement (Young & Chan, 2017). The absorption feature from 0.934 to 1.009 microns observed by the Opportunity Pancam showed a marked downturn in reflectance when gypsum veins were detected due to the H_2O overtone from hydrated calcium sulfate (Farrand et al., 2016). We also observe this downturn with the Torrey gypsum veins in ISEM-E ground truth and AUPE3 data. Late-stage mineral veins can be distinguished across multiple sites with the S950_1000 parameter (Figure 4C1) which shows the degree of positive or negative slope across 950 to 1,000 nm. This spectral range can be indicative of hydrated minerals as it can be used to infer the presence of the H_2O combination band and/or the 3_vOH overtone feature at around 1,000 nm (Rice, Bell III et al. 2013; Rice, Cloutis et al. 2013). However, this feature can occur at different wavelength positions for different minerals; thus, only certain hydrated minerals can be detected, and gypsum is one such mineral. We show in (Figure 4c) that this parameter is also useful to differentiate between features with a similarly high albedo.

5.2. Utility of AUPE, ISEM, and CLUPI for Strategic Planning

At each field site we have shown that the ExoMars emulator suite is capable of multiscale characterization of tactical targets of interest that may be in the vicinity of the rover. More distant, strategic targets are also able to be investigated which inform longer-term planning and operations. Finer-resolution imagery of these targets can then be requested for targeting with HRC. As an example, the vertical HRC-E mosaic inset in Figure 8c illustrates the HRC resolution available at close range: Rock textures and individual eroding clasts and grains can be seen on the outcrop face, while the HRC-E image inset in Figure 7c illustrates the detail that can be made out for distant targets. There is a tradeoff between higher-resolution imaging and multispectral imaging for long range targets—AUPE3 pixels at this distance are 20 mm per pixel yet enable spectral data to be obtained (for sufficiently large, resolvable objects), while HRC-E allows finer details to be resolved.

The ISEM targeting pattern may also be dictated by information obtained from HRC images—whether a long horizontal scan is needed to capture spectral variability across a wide feature like a ridge or a gridded scan is needed for a compact feature, for example, to distinguish a float rock from the surface it lies on. If the target is too distant and, therefore, the ISEM FOV too large, the strategic target can be flagged and prioritized for future investigation once the working distance has been reduced.

In this way, the incremental gathering of multiscale and multispectral data by this instrument suite allows a wealth of information about the terrain surrounding the rover to be collected which can in turn provide insight into the subsurface material.

5.3. Data Limitations and False Spectral Signatures

For this work, as ISEM-E is able to capture information from 300 to 2,500 nm, AUPE3 spectra were ground-truthed to ISEM-E spectra so that spectral features could be compared regardless of their perceived albedo. When comparing AUPE3 and ISEM-E spectra, a consistent offset exists between datasets due to differences in viewing geometry between the two systems, as discussed in Harris et al. (2015). In terms of spectral shape, the two datasets are consistent with each other (see supporting information). However, once bidirectional reflectance distribution functions (BRDF) are measured for a range of illumination angles this offset can be quantitatively mitigated using a lookup table applied to AUPE3 data.

Due to concentric artifacts in AUPE3s RWAC filters caused by stray light (Harris et al., 2015) a spurious band depth feature was observed at around 900 nm in AUPE3 data which was not present in ISEM-E data. Regions of interest selected off-center did not appear to be as affected and matched well to the ISEM-E ground truth. The stray light causing these concentric artifacts and spurious absorption feature is confined to the design of the AUPE3 optical system and will not be present in the PanCam system.

These concentric artifacts are also very apparent in the S950_1000 slope parameter calculation as they affect both filters at 950 and 1,000 nm to some degree. Stray light affects each RWAC filter differently, which can

introduce incorrect slope calculations as a result of differing reflectance levels. As an example, in the VNIR at Pillow, all spectra, apart from the dark quench rind, show evidence of a negative slope from 950 to 1,000 nm which can be indicative of the presence of the H_2O combination band and/or the $3_\nu OH$ overtone feature at around 1,000 nm (Rice, Bell III et al. 2013; Rice, Cloutis et al. 2013). Free from the effects of stray light, this VNIR data may be used to infer whether an outcrop has been aqueously altered. However, comparison of AUPE3 data with ISEM-E spectra collected as ground truth over the AUPE3 wavelength range suggests that these slopes were false positives: The red spectrum (representing a mineral vein) in Figure 2e was the only ISEM-E spectrum which truly exhibited an absorption feature across this range. In agreement with Rice et al. (2010), we find that the 950–1,000 nm slope parameter alone cannot be used as an effective hydration indicator. This is because (a) the effect of stray light on AUPE3 data means that the slope parameter cannot be considered reliable and (b) most hydrated minerals do not exhibit their H_2O and/or OH absorptions within this wavelength range. This is illustrated in Figure 5c, in which many sites that exhibit a distinct H_2O absorption feature at 1,900 nm plot with a positive S950_1000 slope value.

It is worth noting that the outcrops examined lacked the dust cover typically present globally on Mars. Dust can lessen the spectral variability observed in an image; for example, hydrated outcrops may be covered with anhydrous dust and soil which obscures their spectral signatures. Conversely, false detections of hydrated signatures can result from dust-covered surfaces when viewed at high-emission angles (Rice et al., 2010). Corrections for dust accumulation on the calibration target also need to be modeled and applied (Bell et al., 2006; Kinch et al., 2007, 2015) to ensure correct calibration of spectral data to R* reflectance.

6. Conclusions and Future Work

Individually, instruments in the emulator suite offer powerful analysis abilities, but the cross-referencing of their data has allowed for a much richer scope of information to be collected, from which tactical and strategic operational decisions can be made. Through the use of instrument emulators, we have demonstrated that the ExoMars imaging instrument suite will be able to effectively detect and characterize science targets of interest from a range of aqueous environments at a variety of spectral and spatial resolutions. This surface data can be used to augment the knowledge of geologists and instrument analysts and facilitate the prioritization of drill targets which will allow access to pristine subsurface deposits which may contain evidence of life, supporting the astrobiological goals of the ExoMars mission.

Future work will focus on improving the detection and characterization of science targets through the combination of imaging data with structural geological data provided through 3D visualization of the environment using digital elevation models (DEM) created from AUPE3 LWAC and RWAC images and visualized in Pro3D (Barnes et al., 2018). PanCam filter subsets will also be developed that can be used in specific environments to highlight specific spectral trends and assist the PanCam team in making pointing recommendations for other instruments within a tactical, sol-to-sol timeframe.

Acknowledgments
This work was supported by the UK Space Agency (ST/P001297/1 and ST/P001394/1). Cousins also acknowledges the Royal Society of Edinburgh for funding. ExoMars analog suite data are available online (http://exomars.wales). The authors would like to thank Mark Fox-Powell, Arola Moreras Marti, and Aubrey Zerkle for field assistance in Iceland; and Robert Barnes, Matthew Balme, Joel Davis, Peter Fawdon, and Melissa Mirino for their assistance in Utah. Thanks also to reviewers Dr. Melissa Rice and Dr. William Farrand for their comments, which greatly improved this manuscript.

References

Alexander, D. A., Deen, R. G., Andres, P. M., Zamani, P., Mortensen, H. B., Chen, A. C., et al. (2006). Processing of Mars Exploration Rover imagery for science and operations planning. *Journal of Geophysical Research*, *111*, E02S02. https://doi.org/10.1029/2005JE002462

Allender, E. J., Stabbins, R. B., Gunn, M. D., Cousins, C. R., & Coates, A. J. (2018). The ExoMars Spectral Tool (ExoSpec): An image analysis tool for ExoMars 2020 PanCam imagery. Image and Signal Processing for Remote Sensing XXIV, 10789.

Altomare, A., Cuocci, C., Giacovazzo, C., Moliterni, A., & Rizzi, R. (2008). QUALX: A computer program for qualitative analysis using powder diffraction data. *Journal of Applied Crystallography*, *41*(4), 815–817.

Arvidson, R. E., Squyres, S. W., Bell, J. F., Catalano, J. G., Clark, B. C., Crumpler, L. S., et al. (2014). Ancient aqueous environments at Endeavour Crater, Mars. *Science*, *343*(6169), 1248097.

Barnes, D., Battistelli, E., Bertrand, R., Butera, F., Chatila, R., Del Biancio, A., et al. (2006). The ExoMars rover and Pasteur payload Phase A study: An approach to experimental astrobiology. *International Journal of Astrobiology*, *5*(3), 221–241.

Barnes, R., Gupta, S., Traxler, C., Ortner, T., Bauer, A., Hesina, G., et al. (2018). Geological analysis of Martian rover-derived digital outcrop models using the 3-D visualization tool, Planetary Robotics 3-D Viewer—Pro3D. *Earth and Space Science*, *5*, 285–307.

Barnes, D., Wilding, M., Gunn, M, Medwyn Pugh, S., Gethyn Tyler, L., Coates, A., et al. (2011). Multi-spectral vision processing for the ExoMars 2018 mission. In *11th Symposium on Advanced Space Technologies in Robotic and Automation (ASTRA 2012)*.

Barnes, D., Wilding, M., Gunn, M., Tyler, L., Pugh, S., Coates, A., et al. (2011). The PanCam Calibration Target (PCT) and multispectral image processing for the ExoMars 2018 mission. In *EPSC-DPS Joint Meeting 2011*, pp. 289.

Bell, J., Joseph, J., & Sohl-Dickstein, J. (2004). MER/Pancam data processing user's guide. (1.0 ed.) Cornell University.

Bell, J. F., Joseph, J., SohlDickstein, J. N., Arneson, H. M., Johnson, M. J., Lemmon, M. T., & Savransky, D. (2006). In flight calibration and performance of the Mars Exploration Rover Panoramic Camera (Pancam) instruments. *Journal of Geophysical Research*, *111*, E02S03. https://doi.org/10.1029/2005JE002444

Bell, J. F., Maki, J. N., Mehall, G. L., Ravine, M. A., Caplinger, M. A., & the Mastcam-Z Team (2016). Mastcam-Z: Designing a geologic, stereoscopic, and multispectral pair of zoom camerals for the NASA Mars 2020 rover. In *3rd International Workshop on Instrumentation for Planetary Missions*. Abstract 4126.

Bell, J. F., Squyres, S. W., Arvidson, R. E., Arneson, H. M., Bass, D., Blaney, D., et al. (2004b). Pancam multispectral imaging results from the Spirit rover at Gusev Crater. *Science*, *305*(5685), 800–806.

Bell, J. F., Squyres, S. W., Arvidson, R. E., Arneson, H. M., Bass, D., Calvin, W., et al. (2004c). Pancam multispectral imaging results from the Opportunity Rover at Meridiani Planum. *Science*, *306*(5702), 1703–1709.

Bell, J. F., Squyres, S. W., Herkenhoff, K. E., Maki, J. N., Arneson, H. M., Brown, D., et al. (2003). Mars Exploration Rover Athena Panoramic Camera (Pancam) investigation. *Journal of Geophysical Research*, *108*(E12), 8063.

Cannon, K. M., Mustard, J. F., & Salvatore, M. R. (2015). Alteration of immature sedimentary rocks on Earth and Mars: Recording aqueous and surface-atmosphere processes. *Earth and Planetary Science Letters*, *417*, 78–86.

Cloutis, E. A., Asher, P. M., & Mertzman, S. A. (2002). Spectral reflectance properties of zeolites and remote sensing implications. *Journal of Geophysical Research*, *107*(E9), 1–19.

Coates, A. J., Jaumann, R., Griffiths, A. D., Leff, C. E., Schmitz, N., Josset, J.-L., et al. the PanCam Team (2017). The PanCam instrument for the ExoMars rover. *Astrobiology*, *17*(6-7), 511–541.

Cousins, C. R., Gunn, M., Prosser, B. J., Barnes, D. P., Crawford, I. A., Griffiths, A. D., et al. (2012). Selecting the geology filter wavelengths for the ExoMars Panoramic Camera instrument. *Planetary and Space Science*, *71*, 80–100.

Downs, R. T., & Hall-Wallace, M. (2003). The American mineralogist crystal structure database. *American Mineralogist*, *88*, 247–250.

Einarsson, Þ. (1994). *Geology of Iceland: Rocks and landscape*: Mál og menning, Reykavík. p255.

European Space Agency (2018). Oxia Planum favoured for ExoMars surface mission. Online www.esa.int/Our_Activities/Human_Spaceflight/Exploration/ExoMars/Oxia_Planum_favoured_for_ExoMars_surface_mission

Farrand, W. H., Bell III, J. F., Johnson, J. R., Rice, M. S., Jolliff, B. L., & Arvidson, R. E. (2014). Observations of rock spectral classes by the Opportunity rover's Pancam on northern Cape York and on Matijevic Hill, Endeavour Crater, Mars. *Journal of Geophysical Research: Planets*, *119*, 2349–2369. https://doi.org/10.1002/2014JE004641

Farrand, W. H., Bell, J. F., Johnson, J. R., Arvidson, R. E., Crumpler, L. S., Hurowitz, J. A., & Schröder, C. (2008). Rock spectral classes observed by the Spirit Rover's Pancam on the Gusev Crater Plains and in the Columbia Hills. *Journal of Geophysical Research*, *113*, E12S38. https://doi.org/10.1029/2008JE003237

Farrand, W. H., Bell, J. F., Johnson, J. R., Rice, M. S., & Hurowitz, J. A. (2013). VNIR multispectral observations of rocks at Cape York, Endeavour crater, Mars by the Opportunity rover's Pancam. *Icarus*, *225*(1), 709–725.

Farrand, W. H., Bell, J. F., Johnson, J. R., Squyres, S. W., Soderblom, J., & Ming, D. W. (2006). Spectral variability among rocks in visible and near-infrared multispectral Pancam data collected at Gusev crater: Examinations using spectral mixture analysis and related techniques. *Journal of Geophysical Research*, *111*, E02S15. https://doi.org/10.1029/2005JE002495

Farrand, W. H., Johnson, J. R., Rice, M. S., Wang, A., & Bell, J. F. (2016). VNIR multispectral observations of aqueous alteration materials by the Pancams on the Spirit and Opportunity Mars Exploration Rovers. *American Mineralogist*, *101*, 2005–2019.

Gillespie, A. R., Kahle, A. B., & Walker, R. E. (1986). Color enhancement of highly correlated images. I. Decorrelation and HSI contrast stretches. *Remote Sensing of Environment*, *20*(3), 209–235.

Grazulis, S., Chateigner, D., Downs, R. T., Yokochi, A. T., Quirós, M., Lutterotti, L., et al. (2009). Crystallography Open Database—An open-access collection of crystal structures. *Journal of Applied Crystallography*, *42*, 726–729.

Grazulis, S., Daskevic, A., Merkys, A., Chateigner, D., Lutterotti, L., Quirós, M., et al. (2012). Crystallography Open Database (COD): An open-access collection of crystal structures and platform for world-wide collaboration. *Nucleic Acids Research*, *40*, D420–D427.

Griffiths, A. D., Coates, A. J., Josset, J.-L., Paar, G., Hofmann, B., Rueffer, P., et al. (2005). The Beagle 2 stereo camera system: Scientific objectives and design characteristics. *Planetary and Space Science*, *53*, 1446–1482.

Grotzinger, J. P., Sumner, D. Y., Kah, L. C., Stack, K., Gupta, S., Edgar, L., et al. (2014). A habitable fluvio-lacustrine environment at Yellowknife Bay, Gale Crater, Mars. *Science*, *343*(6169), 1242777.

Harris, J. K., Cousins, C. R., Gunn, M., Grindrod, P. M., Barnes, D., Crawford, I. A., et al. (2015). Remote detection of past habitability at Mars-analogue hydrothermal alteration terrains using an ExoMars Panoramic Camera emulator. *Icarus*, *252*, 284–300.

Josset, J.-L., Westall, F., Hofmann, B. A., Spray, J., Cockell, C., Kempe, S., et al. (2017). The Close-Up Imager onboard the ESA ExoMars rover: Objectives, description, operations, and science validation activities. *Astrobiology*, *17*(6-7), 595–611. PMID: 28731819.

Kinch, K. M, Bell, J. F., Goetz, J. F., Johnson, J. R., Madsen, M. B., & Sohl-Dickstein, J. (2015). Dust deposition on the decks of the Mars exploration rovers: 10 years of dust dynamics on the panoramic camera calibration targets. *Earth and Space Science*, *2*(5), 144–172.

Kinch, K. M., Sohl-Dickstein, J., Bell, J. F. III, Johnson, J. R., Goetz, W., & Landis, G. A. (2007). Dust deposition on the Mars Exploration Rover Panoramic Camera (Pancam) calibration targets. *Journal of Geophysical Research*, *112*, E06S03. https://doi.org/10.1029/2006JE002807

Korablev, O. I., Dobrolensky, Y., Evdokimova, N., Fedorova, A. A., Kuzmin, R. O., Mantsevich, S. N., et al. (2017). Infrared spectrometer for ExoMars: A mast-mounted instrument for the rover. *Astrobiology*, *17*(6-7), 542–564.

Malin, M. C., Caplinger, M. A., Edgett, K. S., Ghaemi, F. T., Ravine, M. A., Schaffner, J. A., et al. (2010). The Mars Science Laboratory (MSL) mast-mounted cameras (Mastcams) flight instruments. In *41st Lunar and Planetary Science Conference*. Abstract 1123.

McKeown, N. K., Bishop, J. L., Noe Dobrea, E. Z., Ehlmann, B. L., Parente, M., Mustard, J. F., et al. (2018). Characterization of phyllosilicates observed in the central Mawrth Vallis region, Mars, their potential formational processes, and implications for past climate. *Journal of Geophysical Research*, *114*, E00D10. https://doi.org/10.1029/2008JE003301

McMahon, S., Bosak, T., Grotzinger, J. P., Milliken, R. E., Summons, R. E., Daye, M., et al. (2018). A field guide to finding fossils on Mars. *Journal of Geophysical Research: Planets*, *123*, 1012–1040. https://doi.org/10.1029/2017JE005478

Michalski, J. R., Bibring, J.-P., Poulet, F., Loizeau, D., Mangold, N., Dobrea, E. N., et al. (2010). The Mawrth Vallis region of Mars: A potential landing site for the Mars Science Laboratory (MSL) mission. *Astrobiology*, *10*(7), 687–703.

Murchie, S. L., Mustard, J. F., Ehlmann, B. L., Milliken, R. E., Bishop, J. L., McKeown, N. K., et al. (2009). A synthesis of Martian aqueous mineralogy after 1 Mars year of observations from the Mars Reconnaissance Orbiter. *Journal of Geophysical Research*, *114*, E00D06. https://doi.org/10.1029/2009JE003342

NASA (2017). Mastcam special filters help locate variations ahead. Online, www.jpl.nasa.gov/spaceimages/details.php?id=PIA22065

Nachon, M., Clegg, S. M., Mangold, N., Schröder, S., Kah, L. C., Dromart, G., et al. (2014). Calcium sulfate veins characterized by ChemCam/Curiosity at Gale crater, Mars. *Journal of Geophysical Research: Planets*, *119*, 1991–2016. https://doi.org/10.1002/2013JE004588

Nimmo, F., & Tanaka, K. (2005). Early crustal evolution of Mars. *Annual Review of Earth and Planetary Sciences*, *33*(1), 133–161.

Parente, M., Bishop, J. L., & Bell, J. F. (2009). Spectral unmixing for mineral identification in pancam images of soils in Gusev crater, Mars. *Icarus*, *203*(2), 421–436.

Pelkey, S. M., Mustard, J. F., Murchie, S., Clancy, R. T., Wolff, M., Smith, M., et al. (2007). CRISM multispectral summary products: Parameterizing mineral diversity on Mars from reflectance. *Journal of Geophysical Research*, *112*, E08S14. https://doi.org/10.1029/2006JE002831

Quantin-Nataf, C., Thollot, P., Carter, J., Mandon, L., & Dehouck, E. (2018). The unique and diverse record of Noachian aqueous activity in Oxia Planum, Mars. In *49th Lunar and Planetary Science Conference*. Abstract 2562.

Reed, I. S., & Yu, X. (1990). Adaptive multiple-band CFAR detection of an optical pattern with unknown spectral distribution. *IEEE Transactions on Acoustics, Speech and Signal Processing*, *38*(10), 1760–1770.

Reid, R. J., Smith, P. H., Lemmon, M., Tanner, R., Burkland, M., Wegryn, E., et al. (1999). Imager for Mars Pathfinder (IMP) image calibration. *Journal of Geophysical Research*, *104*(E4), 8907–8925.

Rice, M. S., Bell, J. F., Cloutis, E. A., Wang, A., Ruff, S. W., Craig, M. A., et al. (2010). Silica-rich deposits and hydrated minerals at Gusev Crater, Mars: Vis-NIR spectral characterization and regional mapping. *Icarus*, *205*(2), 375–395.

Rice, M., Bell III, J. F., Arvidson, R., Farrand, W., Johnson, J., Rice Jr, J., et al. (2013). Mapping hydration with the Mars Exploration Rover (MER) pancam instruments: Recent Results from opportunity at Endeavour crater. EGU General Assembly, Vienna, Austria.

Rice, M. S., Cloutis, E. A., Bell, J. F., Bish, D. L., B.H., H., Mertzman, S. A., et al. (2013). Refectance spectra diversity of silica-rich materials: Sensitivity to environment and implications for detections on Mars. *Icarus*, *223*(1), 499–533.

Squyres, S. W., Arvidson, R. E., Bell, J. F., Calef, F., Clark, B. C., Cohen, B. A., et al. (2012). Ancient impact and aqueous processes at Endeavour crater, Mars. *Science*, *336*(6081), 570–576.

The ExoMars 2018 Landing Site Selection Working Group (LSSWG) (2014). Recommendation for the narrowing of ExoMars 2018 Landing sites (*EXM-SCI-LSS-ESA/IKI-004*): European Space Agency.

Vago, J. L., Westall, F., Pasteur Instrument Teams, Landing Site Selection Working Group, Other Contributors, Coates, A. J., Jaumann, R., Korablev, O., Ciarletti, V., et al. the ExoMars Project Team (2017). Habitability on early Mars and the search for biosignatures with the ExoMars rover. *Astrobiology*, *17*(6-7), 471–510.

Viviano-Beck, C. E., Seelos, F. P., Murchie, S. L., Kahn, E. G., Seelos, K. D., Taylor, H. W., et al. (2014). Revised CRISM spectral parameters and summary products based on the currently detected mineral diversity on Mars. *Journal of Geophysical Research: Planets*, *119*, 1403–1431. https://doi.org/10.1002/2014JE004627

Warner, N. H., & Farmer, J. D. (2010). Subglacial hydrothermal alteration minerals in Jökulhlaup deposits of southern Iceland, with implications for detecting past or present habitable environments on Mars. *Astrobiology*, *10*(5), 523–547.

Wellington, D. F., Bell III, J. F., Johnson, J. R., Kinch, K. M., Rice, M. S., Godber, A., et al. The MSL Science Team (2017). Visible to near-infrared MSL/Mastcam multispectral imaging: Initial results from select high-interest science targets within Gale Crater, Mars. *American Mineralogist*, *102*, 1202–1217.

Williams, R. M. E., Irwin, R. P. I., Zimbelman, J. R., Chidsey Jr., T. C., Eby, D. E., Garry, W. B., & Bleacher, J. E. (2011). Field guide to exhumed paleochannels near Green River, Utah: Terrestrial analogs for sinuous ridges on Mars. Analogs for Planetary Exploration, Geological Society of America, Special Paper 483.

Young, B. W., & Chan, M. A. (2017). Gypsum veins in Triassic Moenkopi mudrocks of southern Utah: Analogs to calcium sulfate veins on Mars. *Journal of Geophysical Research: Planets*, *122*, 150–171. https://doi.org/10.1002/2016JE005118